

---

1 **This manuscript is a preprint** and has been submitted for publication in **Environmental Modelling**  
2 **and Software**. Please note that, despite having undergone peer-review, the manuscript has yet to be  
3 formally accepted for publication. Subsequent versions of this manuscript may have slightly different  
4 content. If accepted, the final version of this manuscript will be available via the 'Peer-reviewed  
5 Publication DOI' link on the right-hand side of this webpage. Please feel free to contact any of the  
6 authors; we welcome feedback

---

7

---

# A toolbox to quickly prepare flood inundation models for LISFLOOD-FP simulations

---

Jeison Sosa (1), Chris Sampson (1,2), Andy Smith (1,2), Jeff Neal (1,2), Paul Bates (1,2)

(1) School of Geographical Sciences, University of Bristol, Bristol, BS8 1SS, UK

(2) Fathom Ltd., Engine Shed, Temple Meads, Bristol, BS1 6QH, UK

## Corresponding author

Jeison Sosa

School of Geographical Sciences

University of Bristol

Bristol, UK

Tel: +44 7460 807038

E-mail: [j.sosa@bristol.ac.uk](mailto:j.sosa@bristol.ac.uk)

## Abstract

Hydrodynamic floodplain inundation models have been popular for many years and used extensively in engineering applications. Continental scale flood studies are now achievable using such models due to the development of terrain elevation, hydrography and river width datasets with global coverage. However, deploying flood models at any scale is time-consuming since input data needs to be processed from different sources. Here we present LFPtools, which is an open-source Python package which encompasses most commonly used methods to prepare input data for large scale flood inundation studies using the LISFLOOD-FP hydrodynamic model. LFPtools performance was verified over the Severn basin in the UK where a 1 km flood inundation model was built within 1.45 mins. Outputs of the test case were compared with the official flood extent footprint of a real event and satisfactory model performance was obtained: Hit rate=0.79, False alarm ratio=0.24 and Critical success index=0.63.

## Keywords

Large-scale, continental-scale, modelling, toolbox, hydraulics, flood, LISFLOOD-FP, Python

## Highlights

- LFPtools provides data processing methods to deploy LISFLOOD-FP models.
- LFPtools is written in way that more complex methods can be easily added.
- LFPtools can be used within a sensitivity analysis framework.
- LFPtools is intended for both non-specialist and experienced flood modellers.

47 **Software availability**

48 The toolbox developed in this research is written in Python and built on top of GDAL  
49 (<https://www.gdal.org>), Cython (<http://cython.org/>), Pandas (<https://pandas.pydata.org/>), Numpy  
50 (<http://www.numpy.org/>), xarray (<http://xarray.pydata.org>) and TauDEM  
51 (<http://hydrology.usu.edu/taudem/>). Code and installation instruction are available at  
52 <https://github.com/jsosa/LFPtools>. The toolbox is distributed under the 3-Clause BSD license.

53

54

55

## 56 1 Introduction

57

58 Hydrodynamic models designed to simulate floodplain inundation have been popular for many years  
59 and are widely used in engineering applications. These models, such as TUFLOW (Syme, 1991),  
60 JFLOW (Bradbrook et al., 2004), TRENT (Villanueva and Wright, 2006) and LISFLOOD-FP (Bates et  
61 al., 2010), route water through channels and floodplains following shallow water flow theory.

62

63 Global to continental scale flood studies are being used for insurers, multi-national corporations, NGOs  
64 and national governments. They have been made possible as a result of the appearance of global  
65 coverage datasets of terrain elevation (Farr et al., 2007; Tadono et al., 2015; Yamazaki et al., 2017;  
66 Rizzoli et al., 2017, Wessel et al., 2018), hydrography (Lehner et al., 2008; Yamazaki et al., 2019) and  
67 river width (Andreadis et al., 2013; Yamazaki et al., 2014; Allen and Pavelsky, 2018). These data sets,  
68 coupled with the parallel development of efficient two-dimensional flood models (Bates et al., 2010,  
69 Neal et al., 2012; Sanders et al., 2010) and advances in computational power (Neal et al., 2018; Lamb  
70 et al., 2009), have led to the implementation of flood inundation studies in data-sparse areas around  
71 the world at very high resolutions ( $10^2$ - $10^3$  m). As consequence, a variety of applications involving flood  
72 hydrodynamic variables —flood extent, water depth, flow velocity, flow discharge— have been explored  
73 (Winsemius et al., 2013; Sampson et al., 2015; Wing et al., 2018; Dottori et al., 2017; Alfieri et al., 2018;  
74 Schumann et al., 2016; Lu et al., 2016)

75

76 Building a flood model can be time-consuming since input data need to be processed from a variety  
77 different sources and adapted to a particular user's problem. The increasing quantity, complexity and  
78 resolution of useful datasets imparts an ever-growing burden of knowledge on model developers.  
79 Furthermore, the frequent update cycles of some datasets can cause module builds to go out of date  
80 quickly. Therefore, developing a flood inundation model requires a high level of skill in handling  
81 geographical information using Graphical User Interface (GUI) driven software packages such as  
82 ArcGIS and QGIS. These present a workable solution for the treatment of data, but typically only at  
83 small-scales due to their high demands for computing resource and user intervention. Instead, at  
84 continental-scale command line interface (CLI) software packages are the best candidates for the  
85 preparation of flood inundation models since they provide robustness and computational efficiency. CLI  
86 packages can also be simpler and more streamlined than general GIS software, providing only the  
87 functionality that users need and thus making sophisticated flood inundation modelling more accessible  
88 to specialist users.

89

90 In this paper we present LFPtools, a Python CLI package which attempts to encompass the most  
91 commonly used methods to prepare input data for flood inundation studies using LISFLOOD-FP  
92 (Sampson et al., 2015; Schumann et al., 2013; Hawker et al., 2018) a widely used flood inundation  
93 model. Among the capabilities LFPtools can provide are: DEM upscaling, bank elevation estimation,  
94 bed elevation estimation, river width subtraction and interpolation, elevation smoothing algorithms,  
95 continent basin splitting, and more. Whilst the software has been built specifically for the LISFLOOD-

96 FP model, many of the operations it encodes are useful for a wide range of other flood inundation  
 97 models, especially those operating on regular grids. LFPtools can act as an intermediate platform to  
 98 streamline the preparation of local, continental or global flood inundation studies in different fields by  
 99 bringing ease of use to non-expert users and efficiency to expert ones. For example, new experimental  
 100 studies on hydrological-hydrodynamic modelling, sensitivity analysis (SAFE Toolbox [Pianosi et al.,](#)  
 101 [2015](#); SALib [Herman et al., 2017](#)) will be achievable more straightforwardly. LFPtools is open-source  
 102 and presents a series of tools to estimate the variables required for flood inundation modelling in rapid  
 103 and automated manner. As open-source, users can revise the code, modify or add new methods easily  
 104 and transparently. The tools were verified over the Severn basin where a 1 km flood inundation model  
 105 was built in under 2 minutes on a standard laptop (1.6 GHz Intel Core i5; 8 GB 1600 MHz DDR3).

106

## 107 **2 The flood model LISFLOOD-FP**

108

109 LISFLOOD-FP ([Bates et al., 2010](#)) is a floodplain inundation model which solves the Saint-Venant  
 110 equations at very low computational cost by neglecting the flow advection term, as this is unimportant  
 111 for typical gradually varying and subcritical floodplain flows. The implementation of LISFLOOD-FP Sub-  
 112 Grid ([Neal et al., 2012](#)) extends the two-dimensional model for application to large domain areas where  
 113 channels may be smaller than typical grid resolutions by treating river and floodplain channel networks  
 114 as sub-grid scale features. Sub-grid topographic information such as realistic river width estimates is  
 115 important since it increases model accuracy in terms of water level simulation, wave propagation speed,  
 116 and inundation extent ([Yamazaki et al., 2011](#); [Neal et al., 2012](#)).

117

118 Hydrodynamics in LISFLOOD-FP are solved using a momentum equation derived from the quasi-  
 119 linearized one-dimensional form of the Saint-Venant equation described in Eq. (1) where  $q$  is the flow  
 120 per unit width,  $h$  is the flow depth,  $z$  is the bed elevation,  $g$  is the acceleration due to gravity,  $n$  is the  
 121 Manning's friction coefficient and  $R$  is the hydraulic radius which for wide shallow flows can be  
 122 approximated with the flow depth  $h$ .

123

$$124 \frac{\delta q}{\delta t} + \frac{gh\delta(h+z)}{\delta x} + \frac{gn^2q^2}{R^{4/3}h} = 0 \quad (1)$$

125

126 The final form of the unit flow at the next time step is obtained by discretising Eq. (1) with respect to the  
 127 time step  $\Delta t$  as described in Eq. (2):

128

$$129 q_{t+\Delta t} = \frac{q_t - gh_t\Delta t \frac{\partial(h_t+z)}{\partial x}}{(1 + gh_t\Delta tn^2q_t/h_t^{10/3})} \quad (2)$$

130

131 The model has been widely used for different applications at small and large scales ([Wilson et al., 2007](#);  
 132 [Biancamaria et al., 2009](#); [Neal et al., 2012](#); [Schumann et al., 2013](#); [Schumann et al., 2016](#); [Alfieri et al.,](#)  
 133 [2014](#); [Sampson et al., 2015](#); [Wing et al., 2018](#)) due its computational speed which is mainly given by

134 neglecting the flow advection in the shallow water equation but also by employing a highly efficient finite  
135 difference numerical solution scheme (de Almeida et al., 2012; de Almeida and Bates, 2013).

136

137 The reader is advised to consult the user manual (Bates et al., 2013) for more information on technical  
138 aspects.

139

### 140 **3 Capabilities and features of LFPtools**

141

142 LFPtools is written in Python and built on top of well-known open-source libraries: GDAL, Cython,  
143 Pandas, Numpy and xarray. The TauDEM toolbox (Tarboton, 2005) is also required for some  
144 functionalities. The library handles I/O operations via well-known file formats such as ESRI Shapefiles  
145 and GeoTIFF.

146

#### 147 **3.1 Floodplain elevations**

148

149 Floodplain elevations define the grid output resolution. Those elevations can be obtained directly using  
150 a Digital Elevation Model (DEM) as-is (i.e. at native resolution). Alternatively, if the native DEM contains  
151 noise, usually derived from instrument error, upscaling the native data will reduce that noise in a coarser  
152 floodplain elevation grid, but may also smooth or lose important small scale elevation features (Neal  
153 et al., 2012; Hawker et al., 2018).

154

155 *lfp-rasterresample* is the program included in the library to upscale DEMs. The program can handle  
156 arrays of any size since it never loads entire arrays on memory but instead it loads a small portion  
157 of the array corresponding to the aggregation kernel to be upscaled. The program receives three inputs:  
158 a high-resolution DEM, a target resolution mask and a searching window threshold. Only cells with  
159 mask=1 will be considered for calculation. The upscaling method is described as follows:

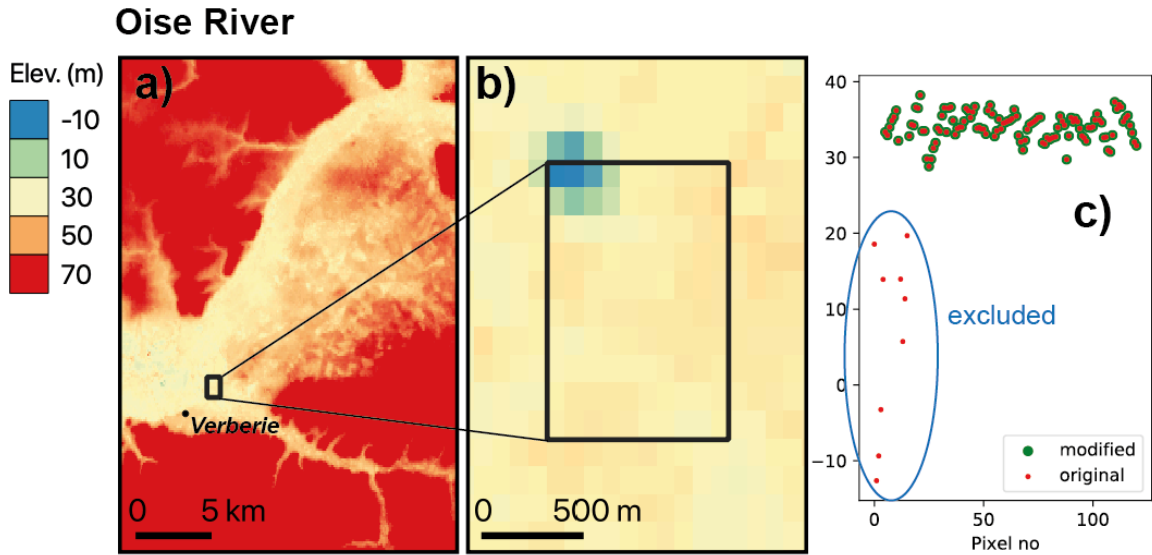
160

- 161 1. A user-defined threshold is applied to a centre cell of the target mask to lump together high-resolution  
162 values.
- 163 2. A modified z-score (Iglewicz and Hoaglin, 1993; based on the median absolute deviation) is  
164 calculated for every DEM cell in the kernel. z-score values larger than 3.5 are identified as outliers  
165 and subsequently removed from the aggregation kernel.
- 166 3. In the aggregation kernel, different reduction algorithms can be applied (e.g., mean, min, meanmin).  
167 'meanmin' is an interesting reduction method which averages the minimum and mean values from  
168 the kernel and emphasises topographic valleys in the calculation. Important to mention that more  
169 reduction algorithms can be easily added in the source code by users should they be required.

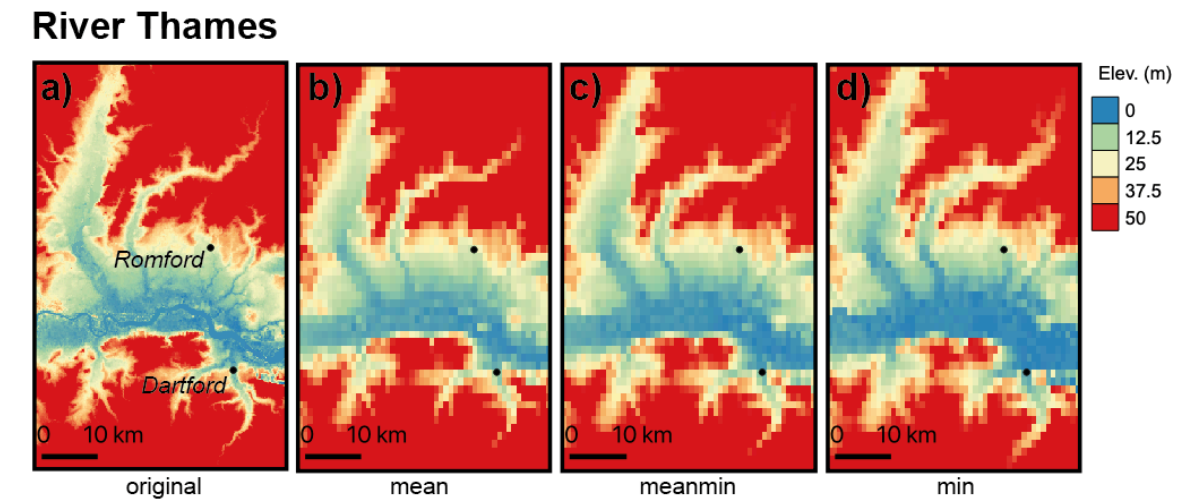
170

171 Step 2 is important to consider since native DEMs might present irregularities in some places. For  
172 example, in development testing a disagreement was found in the aggregation kernel for a target cell  
173 in the Seine River using the native ~90 m resolution MERIT DEM. In particular, some strong negative

174 values (~-10 m) were found in an area where the typical topographic elevation was ~30 m (See Fig. 1).  
 175 The automatic detection algorithm in step 2 prevents inclusion of these values before step 3.  
 176  
 177 Different aggregation methods from Step 3 are compared for a small part of the River Thames using  
 178 the toolbox in Fig. 2.  
 179



180  
 181 **Figure 1:** Outlier detection procedure: a) original 90 m resolution DEM and aggregation kernel (in  
 182 black), b) zoom-in at aggregation kernel (area ~1 km<sup>2</sup>) and c) automatic detection of outliers in kernel  
 183 (in green) points retained for upscaling and (in red) all points.  
 184  
 185



186  
 187 **Figure 2:** Upscaling methods comparison at 1 km resolution: a) original 90 m resolution DEM, b)  
 188 'mean' aggregation, c) 'meanmin' aggregation and d) 'min' aggregation  
 189  
 190  
 191

## 192 3.2 Channel widths

193

194 LISFLOOD-FP Sub-Grid needs several input variables to run a flood simulation, one of which is river  
195 width estimates at every cell in the river network. With the appearance of global river width data sets  
196 based on remote sensing techniques (GWD-LR Yamazaki et al., 2014; GRWL Allen and Pavelsky 2018)  
197 and empirical formulations (Andreadis et al., 2013) it is now feasible to use these data sets as width  
198 sources in flood studies for data-sparse regions.

199

200 Global river width databases may have some degree of geolocation shift in relation to the corresponding  
201 rivers extracted from hydrography databases making them difficult to use in their native format. This  
202 problem may appear if these databases are derived from different sources or due to resolution  
203 dissimilarity; for example, DEM derived river networks and remotely sensed open water locations.  
204 Commonly, a nearest neighbour function in a searching window is used to assign the nearest value  
205 from a river width database to a river cell in a flood study. However, there might be cases where the  
206 searching window is too small and no width values are found, in this case increasing the window size  
207 is not an appealing option since it might result in an incorrect river width assignment from a tributary.  
208 Instead, it is advisable to use an interpolation with values already assigned. It is important to note that  
209 leaving a river cell with no width assigned is a critical issue since LISFLOOD-FP Sub-Grid cannot  
210 perform calculations on river cells with zero width.

211

212 LFPtools includes a routine (*lfp-getwidths*) to automatically assign width values to river cells, it works in  
213 the following way:

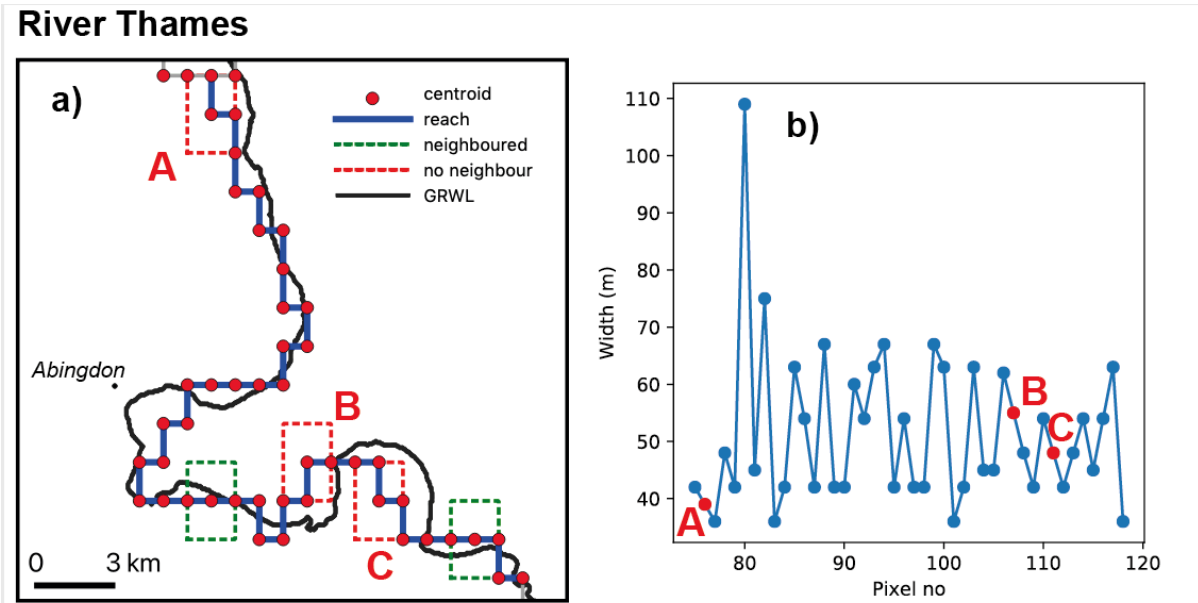
214

- 215 1. River cell widths are assigned based on the nearest-neighbour within a searching window.
- 216 2. If no width value is assigned from the source database, the missing value is automatically  
217 interpolated with values already assigned.

218

219 Fig. 3 shows an example of three river cells with widths unassigned due to the searching window size  
220 problem. Fig. 3a shows a river reach (blue) at ~1 km, red dots are centroids of river cells and the black  
221 solid line is river vector from the GRWL database (~30 m). From the figure only three points (A, B, C)  
222 were not able to find an appropriate width value in their neighbourhood (red dash line), those values  
223 were automatically calculated by interpolation in *lfp-getwidths* see Fig. 3b





225

226

227

228

229

230

231

**Figure 3:** River widths assignment: **a)** Example showing three river cells unassigned due to small size in searching window at locations A, B and C and **b)** (in blue) width values that yield in the searching window (in red) width values interpolated.

### 232 3.3 Bank elevations

233

234

235

236

237

238

The LISFLOOD-FP Sub-Grid uses the DEM elevation as the bank height elevations, which when combined with the channel bed elevation defines the channel bankfull depth. It is therefore recommended to recalculate the bank height elevations to get better estimates because of the critical role this value plays in flooding simulations.

239

240

241

242

243

244

245

246

If a native resolution DEM is used, bank height elevations are self-defined. However, if a coarser resolution model is created, high-resolution cell aggregation is required. *lfp-getbankelevs* reads a target river network mask (mask=1 will be considered for calculation), a high-resolution DEM, and a searching window threshold to aggregate cells and apply a reduction algorithm (nearest, mean, min, meanmin). Resulting elevations might contain irregularities that may result in model instabilities caused by local supercritical flows and flow blocking effects if the channel bed follows the banks. Those irregularities can be solved by applying a smoothing algorithm along the river.

247 LFPtools includes a routine (*lfp-fixelevs*) which includes two approaches to deal with this problem:

248

249

250

1. Adjust bank heights by minimising the amount of modifications following the method developed by Yamazaki et al., (2012). This algorithm removes all the pits in the spaceborne DEM caused by

251 vegetation canopies, sub-pixel sized structures, and random radar speckles while minimizing the  
252 amount of modification required for removing the pits.

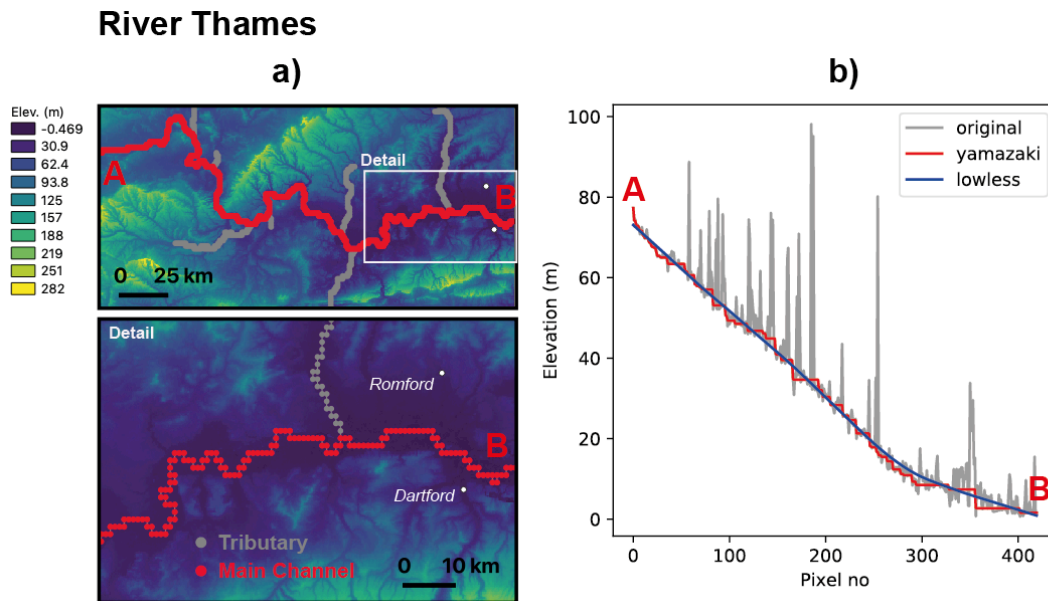
253 2. Apply a weighted local regression (LOWLESS) (Cleveland, 1979) in the downstream direction as in  
254 [Schumann et al., \(2013\)](#).

255

256 Both methods are compared for the main channel of the River Thames, UK in Fig. 4b

257

258



259

260 **Figure 4:** Smoothing method available in LFPtools. These methods were applied to the main channel  
261 of the River Thames: **a)** (in red) main channel of the River Thames and (in grey) tributaries, **b)** (in  
262 grey) original elevation extracted by the nearest-neighbour (in red) Yamazaki's method (in blue)

263

Locally weighted smoothing

264

265

266

### 267 3.4 River depths

268

269 Standard LISFLOOD-FP Sub-Grid treats river cross-sections as rectangular. Due to this fact channel  
270 depths may differ from in-situ river depth surveys. With some calibration this approximation works very  
271 well at large scales producing reasonable results in most places as long as accurate estimations of  
272 bank heights and widths are used. Unlike bank heights and river widths that can be determined from  
273 satellite data, river depths need to be approximated. Two approaches have been proposed to achieve  
274 this goal and are included in the *lfp-getdepths* tool — a simple empirical power law formulation ([Neal et  
275 al., 2012](#)) and the Manning's equation ([Sampson et al., 2015](#)). A user-defined raster (e.g., survey data  
276 on river bathymetry) can also be used to assign depths to cells if none of the previous methods are  
277 used.

278

279 **Power law relationship**

280

281 [Leopold and Maddock \(1953\)](#) derived a series of power law relationships given by Eq. (5), (6) and (7)  
282 where  $W$  is water-surface width,  $Q$  is discharge,  $D$  is mean depth and  $V$  is mean velocity

283

284  $W = aQ^b$  (3)

285  $D = cQ^f$  (4)

286  $V = kQ^m$  (5)

287

288 It is straightforward to equate Eq. (3) and (4) to obtain Eq. (6)

289

290  $D = \left(\frac{c}{af/b}\right)W^{f/b}$  (6)

291

292 where  $(a, b, c, f)$  are empirical values depending on the geomorphology of the bed. Sometimes it is  
293 preferred to use only one pair of constants  $(r, p)$  as in Eq. (7). See [Hey and Thorne \(1986\)](#) for empirical  
294 values for gravel-bed rivers in the UK.

295

296  $D = rW^p$  (7)

297

298

299 **Manning's equation**

300

301 The Manning's equation for a rectangular channel is described by Eq. (8) where  $A$  is the cross-section  
302 area expressed as  $A = WD$  with  $W$  width and  $D$  depth,  $R$  is the hydraulic radius  $R = A/(W + 2D)$ ,  $S$  is  
303 the channel cell slope—it can be calculated via *lfp-slopes* or directly extracted from an external data  
304 set ([Cohen et al., 2018](#))— $n$  is the Manning's coefficient and  $Q_{bf}$  is the bankfull flow.

305

306  $Q_{bf} = \frac{AR^{2/3}S^{1/2}}{n}$  (8)

307

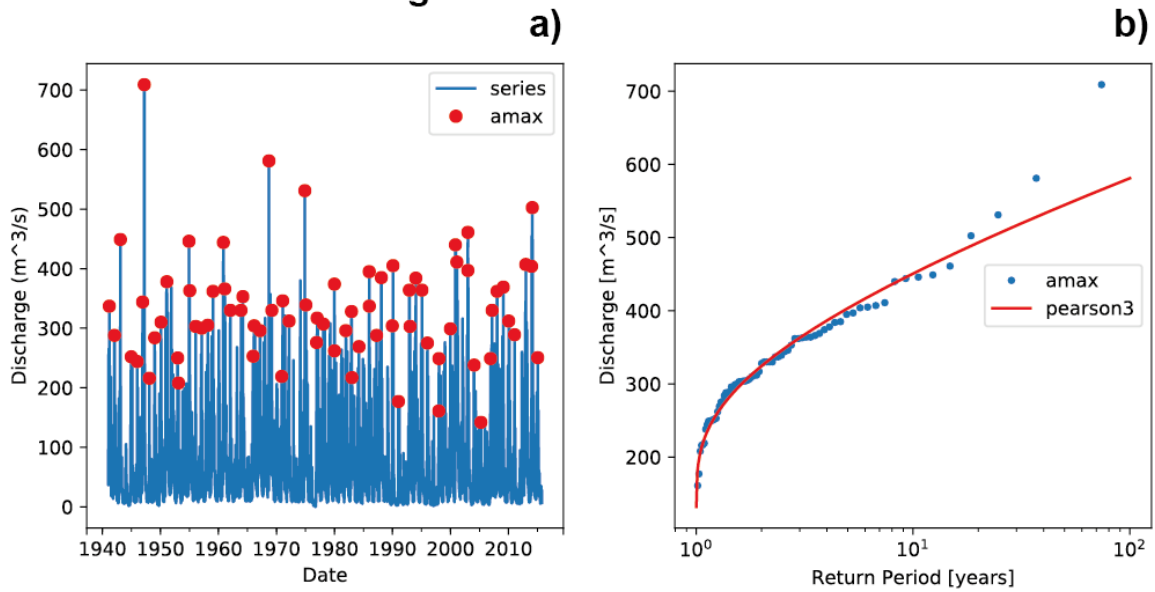
308 The Manning's equation considers bankfull flow  $Q_{bf}$  as a known variable, however it is not always the  
309 case. If not measured in the field, bankfull flow is usually estimated by fitting a statistical distribution on  
310 the annual flow peaks of a streamflow time series where bankfull conditions occur at return periods of  
311 1.5-2 years ([Schneider et al., 2011](#)). Fig. 5 shows the aforementioned procedure for the Kingston  
312 gauging station from the National River Flow Archive (NRFA) on the River Thames, UK.

313

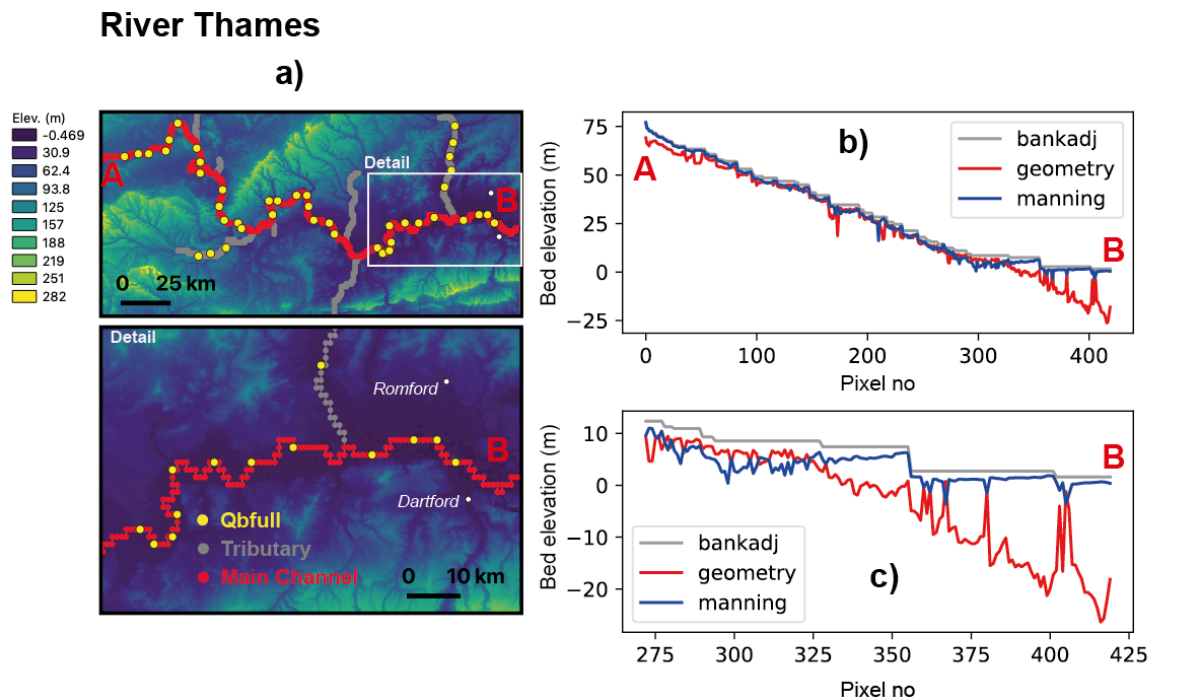
314 A comparison between the Power law relationship and Manning's equation is presented for the River  
315 Thames in Fig. 6. Bankfull flow (yellow dots) was obtained by subtracting the 2-year return period in a  
316 Pearson Type III distribution fitted on the annual maxima time series derived by means of a 24-year

317 streamflow reanalysis from the European Forecasting Awareness System (EFAS) (Thielen et al., 2009).  
 318 River width estimates used in Eq. (7) were obtained from the GRWL database using *lfp-getwidths*. At  
 319 locations where no-bankfull width is available, the nearest bankfull value was assigned. Fig 6c shows  
 320 (in grey) bank elevations after smoothing in the main channel, (in blue) bed elevations (i.e., bank  
 321 elevation - depth) using the Manning's Eq. (8) and (in red) using the power law relationship Eq. (7). A  
 322 zoom for the downstream section is shown in Fig 6d and reveals considerable differences in the delta  
 323 area.  
 324  
 325

### River Thames at Kingston



326  
 327 **Figure 5:** Observed river discharge in the River Thames at Kingston Station. Bankfull was estimated  
 328 by fitting a statistical distribution on the annual maxima and retrieving the discharge value for the 2-yr  
 329 return period: **a)** annual maxima between 1940-2015 (red dots). **b)** Pearson Type III distribution fitted  
 330 on the annual maxima (red line), here the distribution parameters were estimated via L-moments. This  
 331 figure was generated by using the *hydrouils* library (Sosa, 2018).



333

334

335

336

337

338

339

340

### 3.5 Continental tools

341

342

343

344

345

346

347

348

349

350

351

352

353

354

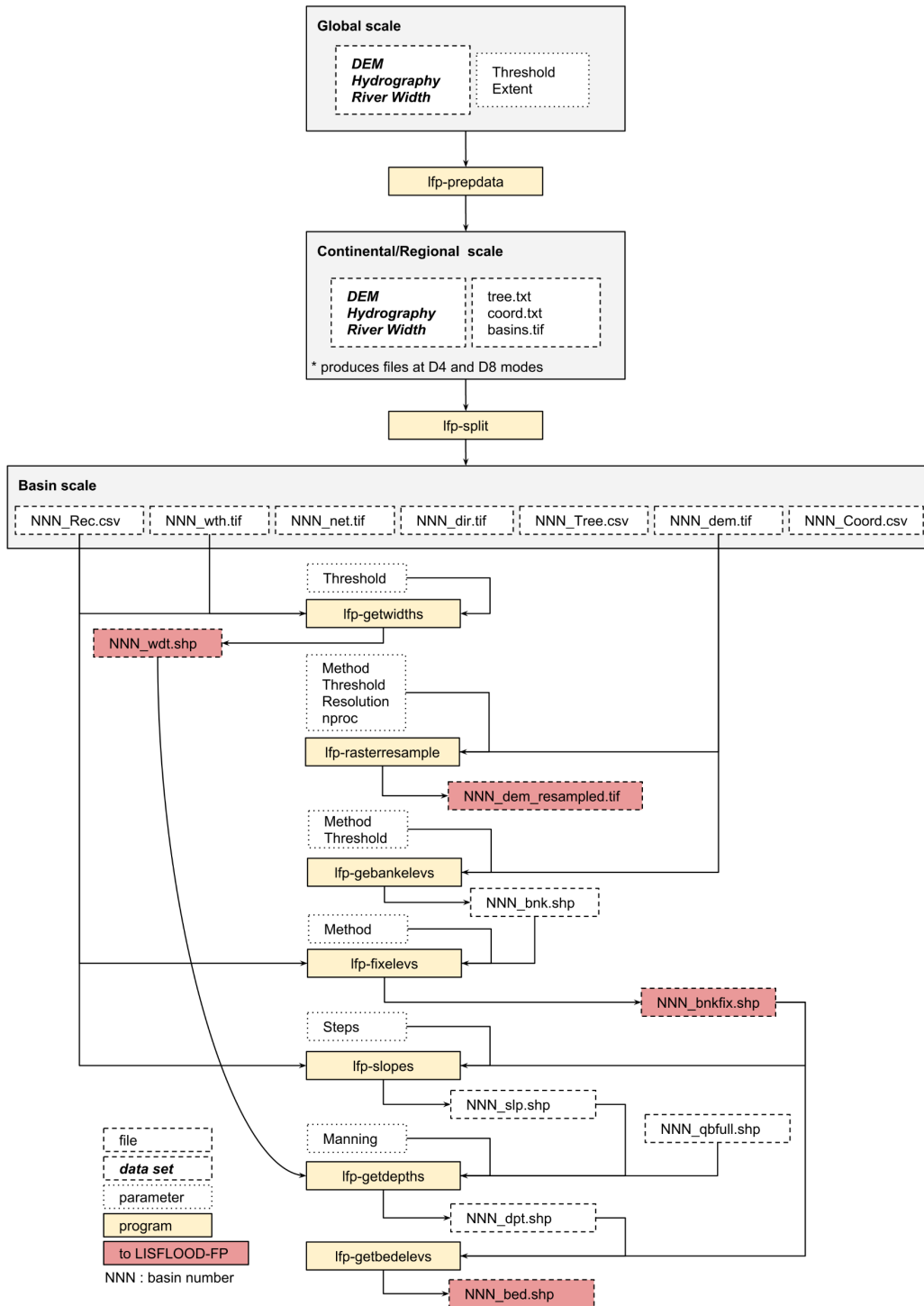
355

**Figure 6:** River depth estimation using hydraulic geometry equations and Manning's equation: **a)** River Thames (in red) tributaries (in grey), **b)** depth estimation via hydraulic geometry (in red) and Manning's equation (in blue) for the lower part of the River Thames and **c)** zoom-in delta area of the River Thames

The library includes two programs designed to automate delineation of basins within large regions *lfp-prepdata* and *lfp-split*.

*lfp-prepdata* incorporates a subroutine to clip global data sets of DEM, hydrography and river width based on a user-defined extent. Thereafter, a user-defined threshold is applied to the flow accumulation area (or upslope drainage area) to define a river network. The TauDEM toolbox (Tarboton, 2005) is used to generate a network topological connectivity for the whole area and to delineate basins within the region (NNN\_Tree.csv, NNN\_Coord.csv and NNN\_Rec.csv in Fig. 7). The routine also includes a function to convert D8 connected river networks to D4 connectivity based on the flow directions map given by the hydrography. *lfp-split* breaks up the region into individual basins with a basin-number associated. Folders are created with a basin-number and each of them contains clipped data associated with that basin. After basin required data is split in this way the tools described in Sections 3.1-3.4 can be applied. Fig. 7 shows a flowchart describing how the tools can connect to each other to automatically build models at continental-scale.

## LFPtools flowchart



356  
357  
358  
359  
360  
361

**Figure 7:** Flowchart using LFPtools for continental-scale studies. Command-line tools are presented in yellow boxes, white dashed boxes represent input data sets and white dotted boxes free parameters. Outputs to LISFLOOD-FP are coloured in red.

362 **3.6 Usage**

363

364 In order to facilitate the use of the tools LFPtools can be called via command-line, however if preferred  
365 it can also be imported as a Python module. All tools can be invoked via the command line by typing  
366 the name of the tool followed by the -i keyword and the name of the configuration file:

367

368 \$ lfp-getwidths -i config.txt

369

370 where the configuration file 'config.txt' is a text file containing a [tool-name] header followed by  
371 variable=argument entries. Input variable descriptions are specified when typing the name of the tool  
372 in the command-line followed by the -h keyword: \$ lfp-getwidths -h

373

374 LFPtools can be imported as a Python module as follows:

375

376 import lfp as lfp

377

378 An overview of tools with a brief description is given in Table 1.

379

380

Program	Description
lfp-depths	Get estimates of depth
lfp-fixelevs	Smooth elevations
lfp-getbankelevs	Retrieve bank elevations
lfp-slopes	Estimate slopes in a river network
lfp-getwidths	Retrieve river widths
lfp-rasterresample	Upscale a high-resolution DEM into a user-defined resolution
lfp-split	Breaks up a study area in individual basins with a basin number associated
lfp-prepdata	Clip global data sets given a user-defined extent and threshold. The threshold is used to define a river network based on the upslope area

381

382

**Table 1:** Summary of programs in LFPtools

383

384

385

386

387

388

389 **4 A flood inundation model for the Severn River in England, UK**

390

391 LFPTools was used to build a flood inundation model for the Severn river basin in the UK. A one-month  
 392 simulation (April 1998) was undertaken in order to capture an observed flood event that happened  
 393 during this period. An additional one month ‘warm-up’ period was included to bring the model into a  
 394 hydraulic steady state condition prior to the commencement of the April 1998 period. The model was  
 395 built from LIDAR-based terrain data (at 90 m resolution) where the floodplain terrain was upscaled to 1  
 396 km resolution using the ‘mean’ aggregation method and removing outliers. Bank heights were defined  
 397 using the ‘nearest neighbour’ method. River channels were explicitly represented using HydroSHEDS  
 398 (Lehner et al., 2008) as input hydrography at 1 km resolution. Channel widths were retrieved from the  
 399 GRWL database while river depths were estimated through the hydraulic geometry method (Eq. 5) with  
 400  $r = 0.12$  and  $p = 0.78$ . The model was forced using daily gauged flows from the UK National River Flow  
 401 Archive (NRFA) for the simulation period mentioned before. Data sources used in this study are briefly  
 402 described in Table 2.

403

Data set	Description	Source
LIDAR DTM	Composite at 1 m resolution	Data available at data.gov.uk
HydroSHEDS	Hydrography at 1 km resolution	Lehner et al., 2018. Data available at hydrosheds.org
GRWL	Landsat-based global river width database at 30 m resolution	Allen and Pavelsky, 2018. Data available at <a href="https://zenodo.org/record/1297434">https://zenodo.org/record/1297434</a>
NRFA	Streamflow data from gauge stations	Data available at nrfa.ceh.ac.uk
Recorded Flood Outlines for UK	Records of historic flooding from rivers, the sea, groundwater and surface water	Data available at data.gov.uk

404

405 **Table 2:** Data sets used to build the flood inundation model in the Severn river basin

406

407 Resulting water depths from LISFLOOD-FP at 1 km resolution were subsequently downscaled onto 90  
 408 m resolution using an algorithm similar to Schumann et al., 2014. In particular, the algorithm takes water  
 409 surface elevation (WSE) at 1 km resolution and subtracts its corresponding 90 m DEM values. From  
 410 this arithmetic operation, a grid at 90 m resolution is created with positive values representing the water  
 411 depth (wet cells) whilst negative values (dry cells) are replaced with nodata values.

412

413 The performance of flood model in the Severn river basin in terms of flood extent was quantified using  
 414 three scores: Hit rate (H), Falsa alarm ratio (F) and Critical success index (C). *H* tests the tendency of  
 415 the model towards underprediction and can range from 0 (none of the wet benchmark data is wet model  
 416 data) to 1 (all of the wet benchmark data are wet model data). *F* examines the tendency of the model

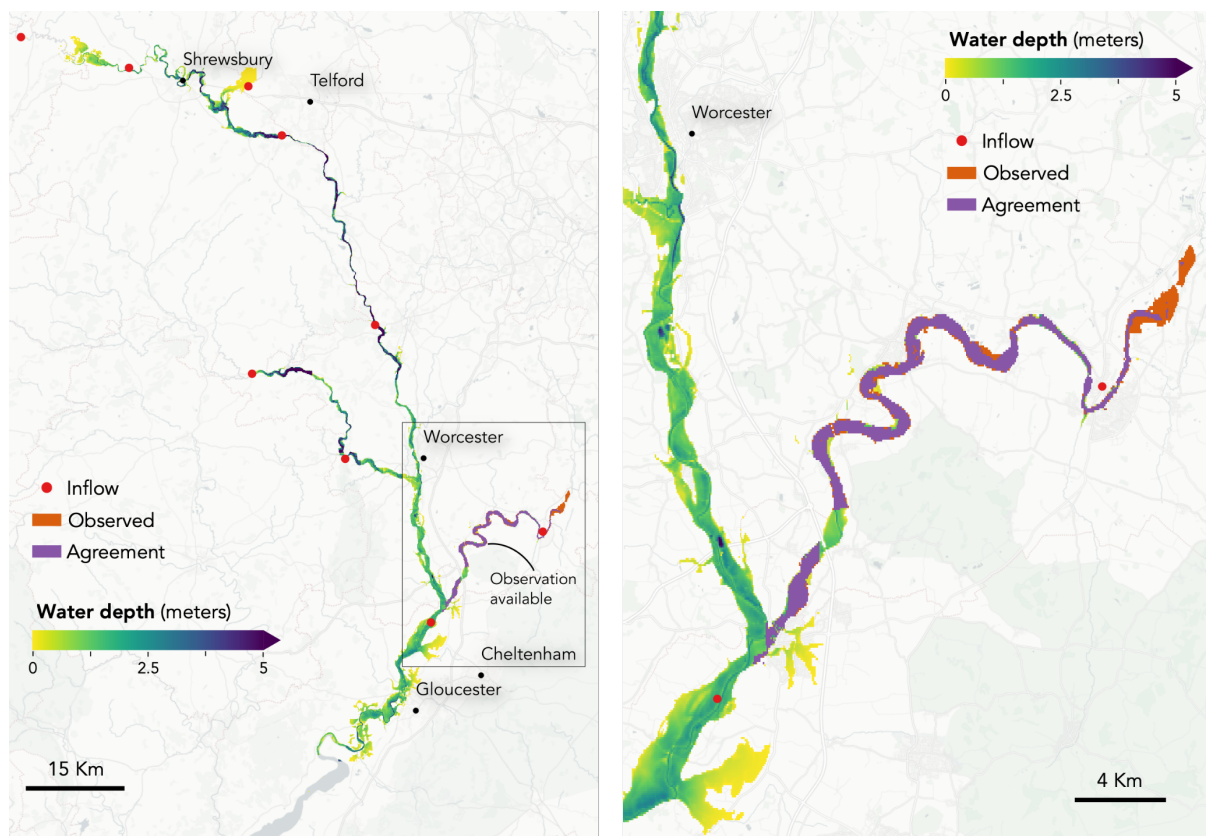


417 towards overprediction and can range from 0 (no false alarms) to 1 (all false alarms).  $C$  accounts for  
418 both overprediction and underprediction and can range from 0 (no match between modelled and  
419 benchmark data) to 1 (perfect match between modelled and benchmark data). A detailed explanation  
420 of these scores is available in Wing et al., 2017.

421

422 Simulated water depth results for the 15<sup>th</sup> April 1998 are shown in Fig. 8. From the figure is clear that  
423 in most places water remains in the channel and where water elevations exceed bankfull heights water  
424 spreads onto the floodplains. Simulated water depth on the 15<sup>th</sup> April 1998 were compared with the  
425 official event footprint from the English Environment Agency (EA) and the 'Agreement' between both  
426 flood extents are presented in the Fig. 8 right-hand panel. The 'Agreement' in Fig. 8 refers to areas in  
427 the map where the EA flood extent and the simulated flood extent overlap each other. In terms of flood  
428 extent, the model obtained satisfactory comparison scores against observations:  $H=0.79$ ,  $F=0.24$  and  
429  $C=0.63$ . Example files are available at the LFPtools web repository.

430



431

432 **Figure 8:** Flood inundation model prepared for the Severn basin in England, UK during the flood  
433 event of April-1998. The event was compared with official footprint of the event (orange). The  
434 agreement between the model and the output is also shown (purple). Note that the observed data  
435 only cover limited portions of the model domain which are not contiguous. In areas with no observed  
436 data we simply plot the modelled water depth. Also, the moderately low *Hit Rates* occur since the  
437 observed flood extent area is upstream of the inflow point (East of the domain in the right-hand  
438 panel), hence, no forcing data is available to predict water depths in that area.

439

440  
441  
442  
443  
444  
445  
446  
447  
448  
449  
450  
451  
452  
453  
454  
455  
456  
457  
458  
459  
460  
461  
462  
463  
464  
465  
466  
467  
468  
469  
470  
471  
472  
473  
474  
475  
476  
477  
478  
479

## 5 Conclusions

A Python CLI package has been developed to help prepare input data for flood studies carried out using LISFLOOD-FP. The package encompasses the most frequently used methods for flood inundation modelling data preparation, and also facilitates the addition of new ones if desired. LFPtools can be thought of as a platform to streamline the preparation of flood inundation studies in different fields by bringing ease of use to non-expert users and efficiency to expert ones. It is built on top of the state-of-the-art Python libraries to handle large sets of data and it is in active development. It is important to mention that these tasks could be done in a GIS package, but only with quite extreme difficulty and for small data arrays. The tasks performed by LFPTools are generic for structured grids and can be used to prepare input data sets for any hydraulic model.

LFPtools programs were verified in the UK's Severn basin on a model built at 1 km resolution using publicly available data sets only. The test basin was used to simulate the event of April 1998 and results are presented in Fig. 8. From the figure it is clear that most of the water is kept in channels with some places inundated suggesting a normal hydrodynamic behaviour. After comparison, the model obtained satisfactory scores against the official event footprint:  $H=0.79$ ,  $F=0.24$  and  $C=0.63$ . It is important to mention that the Severn scenario was used only to broadly test the tools and not to simulate the real event to an engineering standard.

The Severn river basin used in this study is only a small example on how the tools can be employed and the tools have been designed so they can be integrated within a framework to build continental to global scale studies. For example, LFPtools can be used within a modelling framework to build a continental-scale flood hindcast or reanalysis, a modelling framework of continental-scale flood extent for an early warning system or even within a framework to predict flood inundation variables (flood extent, water depth, etc) in a climate change context.

Global to continental scale models are being used by insurers, multi-national corporations, NGOs and national governments to tackle problems such as rapid flood disaster response, urban planning and climate change adaptation. Thus, flood models at such scales are important decision making tools and building them demands great effort to research scientists. We envisage that this innovative set of tools will help to significantly reduce these costs.

## Acknowledgments

J.S. received funding from the European Union's Horizon 2020 research and innovation programme under the Marie Skłodowska-Curie grant agreement No. 676027. P.B. was supported by a Leverhulme Research Fellowship and a Wolfson Research Merit Award from the Royal Society. The authors would like to thank Gemma Coxon for providing the NRFA data.

480 **References**

481

482 Alfieri, L., Dottori, F., Betts, R., Salamon, P., Feyen, L., 2018. Multi-Model Projections of River Flood  
483 Risk in Europe under Global Warming. *Climate* 6, 6. <https://doi.org/10.3390/cli6010006>

484

485 Alfieri, L., Salamon, P., Bianchi, A., Neal, J., Bates, P., Feyen, L., 2014. Advances in pan-European  
486 flood hazard mapping. *Hydrol Process* 28, 4067–4077. <https://doi.org/10.1002/hyp.9947>

487

488 Allen, G.H., Pavelsky, T.M., 2018. Global extent of rivers and streams. *Science*.  
489 <https://doi.org/10.1126/science.aat0636>

490

491 Andreadis, K.M., Schumann, G.J.-P., Pavelsky, T., 2013. A simple global river bankfull width and  
492 depth database: Data and Analysis Note. *Water Resour Res* 49, 7164–7168.  
493 <https://doi.org/10.1002/wrcr.20440>

494

495 Bates, P., Trigg, M., Neal, J., Dabrowa, A., 2013. LISFLOOD-FP user manual. School of  
496 Geographical Sciences, University of Bristol, UK.

497

498 Bates, P.D., Horritt, M.S., Fewtrell, T.J., 2010. A simple inertial formulation of the shallow water  
499 equations for efficient two-dimensional flood inundation modelling. *J Hydrol* 387, 33–45.  
500 <https://doi.org/10.1016/j.jhydrol.2010.03.027>

501

502 Biancamaria, S., Bates, P.D., Boone, A., Mognard, N.M., 2009. Large-scale coupled hydrologic and  
503 hydraulic modelling of the Ob river in Siberia. *J Hydrol* 379, 136–150.  
504 <https://doi.org/10.1016/j.jhydrol.2009.09.054>

505

506 Bradbrook, K.F., Lane, S.N., Waller, S.G., Bates, P.D., 2004. Two dimensional diffusion wave  
507 modelling of flood inundation using a simplified channel representation. *Intl. J. River Basin*  
508 *Management* 2, 211–223. <https://doi.org/10.1080/15715124.2004.9635233>

509

510 Cleveland, W.S., 1979. Robust Locally Weighted Regression and Smoothing Scatterplots. *Journal of*  
511 *the American Statistical Association* 74, 829–836.  
512 <https://doi.org/10.1080/01621459.1979.10481038>

513

514 Cohen, S., Wan, T., Islam, M.T., Syvitski, J.P.M., 2018. Global river slope: A new geospatial dataset  
515 and global-scale analysis. *J Hydrol* 563, 1057–1067. <https://doi.org/10.1016/j.jhydrol.2018.06.066>

516

517 de Almeida, G.A.M., Bates, P., 2013. Applicability of the local inertial approximation of the shallow  
518 water equations to flood modeling. *Water Resour Res* 49, 4833–4844.  
519 <https://doi.org/10.1002/wrcr.20366>

520

521 de Almeida, G.A.M., Bates, P., Freer, J.E., Souvignet, M., 2012. Improving the stability of a simple  
522 formulation of the shallow water equations for 2-D flood modeling. *Water Resour Res* 48.  
523 <https://doi.org/10.1029/2011WR011570>

524

525 Dottori, F., Kalas, M., Salamon, P., Bianchi, A., Alfieri, L., Feyen, L., 2017. An operational procedure  
526 for rapid flood risk assessment in Europe. *Nat Hazards Earth Syst Sci* 17, 1111–1126.  
527 <https://doi.org/10.5194/nhess-17-1111-2017>

528

529 Farr, T.G., Rosen, P.A., Caro, E., Crippen, R., Duren, R., Hensley, S., Kobrick, M., Paller, M.,  
530 Rodriguez, E., Roth, L., Seal, D., Shaffer, S., Shimada, J., Umland, J., Werner, M., Oskin, M.,  
531 Burbank, D., Alsdorf, D., 2007. The Shuttle Radar Topography Mission. *Rev Geophys* 45.  
532 <https://doi.org/10.1029/2005RG000183>

533

534 Hawker, L., Rougier, J., Neal, J., Bates, P., Archer, L., Yamazaki, D., 2018. Implications of Simulating  
535 Global Digital Elevation Models for Flood Inundation Studies. *Water Resour Res* 54, 7910–7928.  
536 <https://doi.org/10.1029/2018WR023279>

537

538 Herman, J., Usher, W., 2017. SALib: An open-source Python library for Sensitivity Analysis. The  
539 Journal of Open Source Software 2, 97. <https://doi.org/10.21105/joss.00097>  
540

541 Hey, R.D., Thorne, C.R., 1986. Stable Channels with Mobile Gravel Beds. J Hydraul Eng 112, 671–  
542 689. [https://doi.org/10.1061/\(ASCE\)0733-9429\(1986\)112:8\(671\)](https://doi.org/10.1061/(ASCE)0733-9429(1986)112:8(671))  
543

544 Iglewicz, B. and Hoaglin, D.C., 1993. How to detect and handle outliers (Vol. 16). Asq Press.  
545

546 Lamb, R., Crossley, M., Waller, S., 2009. A fast two-dimensional floodplain inundation model.  
547 Proceedings of the Institution of Civil Engineers - Water Management 162, 363–370.  
548 <https://doi.org/10.1680/wama.2009.162.6.363>  
549

550 Lehner, B., Verdin, K., Jarvis, A., 2008. New Global Hydrography Derived From Spaceborne  
551 Elevation Data. Eos, Transactions American Geophysical Union 89, 93.  
552 <https://doi.org/10.1029/2008EO100001>  
553

554 Leopold, L.B., Maddock Jr., T., 1953. The hydraulic geometry of stream channels and some  
555 physiographic implications (Report No. 252), Professional Paper. Washington, D.C.  
556

557 Lu, X., Zhuang, Q., Liu, Y., Zhou, Y., Aghakouchak, A., 2016. A large-scale methane model by  
558 incorporating the surface water transport: Development of a Methane Model. J Geophys Res  
559 Biogeosci 121, 1657–1674. <https://doi.org/10.1002/2016JG003321>  
560

561 Neal, J., Dunne, T., Sampson, C., Smith, A., Bates, P., 2018. Optimisation of the two-dimensional  
562 hydraulic model LISFOOD-FP for CPU architecture. Environ Model Softw 107, 148–157.  
563 <https://doi.org/10.1016/j.envsoft.2018.05.011>  
564

565 Neal, J., Schumann, G., Bates, P., 2012. A subgrid channel model for simulating river hydraulics and  
566 floodplain inundation over large and data sparse areas. Water Resour Res 48.  
567 <https://doi.org/10.1029/2012WR012514>  
568

569 Pianosi, F., Sarrazin, F., Wagener, T., 2015. A Matlab toolbox for Global Sensitivity Analysis. Environ  
570 Model Softw 70, 80–85. <https://doi.org/10.1016/j.envsoft.2015.04.009>  
571

572 Rizzoli, P., Martone, M., Gonzalez, C., Wecklich, C., Borla Tridon, D., Bräutigam, B., Bachmann, M.,  
573 Schulze, D., Fritz, T., Huber, M., Wessel, B., Krieger, G., Zink, M., Moreira, A., 2017. Generation  
574 and performance assessment of the global TanDEM-X digital elevation model. Isprs J  
575 Photogramm 132, 119–139. <https://doi.org/10.1016/j.isprsjprs.2017.08.008>  
576

577 Sampson, C.C., Smith, A.M., Bates, P.D., Neal, J.C., Alfieri, L., Freer, J.E., 2015. A high-resolution  
578 global flood hazard model. Water Resour Res 51, 7358–7381.  
579 <https://doi.org/10.1002/2015WR016954>  
580

581 Sanders, B.F., Schubert, J.E., Detwiler, R.L., 2010. ParBreZo: A parallel, unstructured grid, Godunov-  
582 type, shallow-water code for high-resolution flood inundation modeling at the regional scale. Adv  
583 Water Resour 33, 1456–1467. <https://doi.org/10.1016/j.advwatres.2010.07.007>  
584

585 Schneider, C., Flörke, M., Eisner, S., Voss, F., 2011. Large scale modelling of bankfull flow: An  
586 example for Europe. J Hydrol 408, 235–245. <https://doi.org/10.1016/j.jhydrol.2011.08.004>  
587

588 Schumann, G.J.-P., Andreadis, K.M., Bates, P.D., 2014. Downscaling coarse grid hydrodynamic  
589 model simulations over large domains. J Hydrol 508, 289–298.  
590 <https://doi.org/10.1016/j.jhydrol.2013.08.051>  
591

592 Schumann, G.J.-P., Neal, J.C., Voisin, N., Andreadis, K.M., Pappenberger, F., Phanthuwongpakdee,  
593 N., Hall, A.C., Bates, P.D., 2013. A first large-scale flood inundation forecasting model: Large-  
594 Scale Flood Inundation Forecasting. Water Resour Res 49, 6248–6257.  
595 <https://doi.org/10.1002/wrcr.20521>  
596

597 Schumann, G.J.-P., Stampoulis, D., Smith, A.M., Sampson, C.C., Andreadis, K.M., Neal, J.C., Bates,  
598 P.D., 2016. Rethinking flood hazard at the global scale. *Geophys Res Lett* 43, 10,249-10,256.  
599 <https://doi.org/10.1002/2016GL070260>  
600

601 Sosa, J., 2018. Hydroutils. <https://doi.org/10.5281/zenodo.1408076>  
602

603 Syme, W.J., 1991. Dynamically Linked Two-dimensional/One-dimensional Hydrodynamic Modelling  
604 Program for Rivers, Estuaries & Coastal Waters (MEngSc thesis). University of Queensland,  
605 Australia.  
606

607 Tadono, T., Takaku, J., Tsutsui, K., Oda, F., Nagai, H., 2015. Status of “ALOS World 3D (AW3D)”  
608 global DSM generation. *Proceeding 2015 IEEE International Geoscience and Remote Sensing*  
609 *Symposium (IGARSS)*, pp. 3822–3825. <https://doi.org/10.1109/IGARSS.2015.7326657>  
610

611 Tarboton, D.G., 2005. Terrain analysis using digital elevation models (TauDEM).  
612

613 Thielen, J., Bartholmes, J., Ramos, M.-H., de Roo, A., 2009. The European Flood Alert System – Part  
614 1: Concept and development. *Hydrol Earth Syst Sci* 13, 125–140. [https://doi.org/10.5194/hess-13-](https://doi.org/10.5194/hess-13-125-2009)  
615 [125-2009](https://doi.org/10.5194/hess-13-125-2009)  
616

617 Villanueva, I., Wright, N.G., 2006. Linking Riemann and storage cell models for flood prediction.  
618 *Proceedings of the Institution of Civil Engineers - Water Management* 159, 27–33.  
619 <https://doi.org/10.1680/wama.2006.159.1.27>  
620

621 Wessel, B., Huber, M., Wohlfart, C., Marschalk, U., Kosmann, D., Roth, A., 2018. Accuracy  
622 assessment of the global TanDEM-X Digital Elevation Model with GPS data. *Isprs J Photogramm*  
623 *139*, 171–182. <https://doi.org/10.1016/j.isprsjprs.2018.02.017>  
624

625 Wilson, M., Bates, P., Alsdorf, D., Forsberg, B., Horritt, M., Melack, J., Frappart, F., Famiglietti, J.,  
626 2007. Modeling large-scale inundation of Amazonian seasonally flooded wetlands. *Geophys Res*  
627 *Lett* 34. <https://doi.org/10.1029/2007GL030156>  
628

629 Wing, O.E.J., Bates, P.D., Sampson, C.C., Smith, A.M., Johnson, K.A., Erickson, T.A., 2017.  
630 Validation of a 30 m resolution flood hazard model of the conterminous United States. *Water*  
631 *Resour Res* 53, 7968–7986. <https://doi.org/10.1002/2017WR020917>  
632

633 Wing, O.E.J., Bates, P.D., Smith, A.M., Sampson, C.C., Johnson, K.A., Fargione, J., Morefield, P.,  
634 2018. Estimates of present and future flood risk in the conterminous United States. *Environ Res*  
635 *Lett* 13, 034023. <https://doi.org/10.1088/1748-9326/aaac65>  
636

637 Winsemius, H.C., Van Beek, L.P.H., Jongman, B., Ward, P.J., Bouwman, A., 2013. A framework for  
638 global river flood risk assessments. *Hydrol Earth Syst Sci* 17, 1871–1892.  
639 <https://doi.org/10.5194/hess-17-1871-2013>  
640

641 Yamazaki, D., Ikeshima, D., Tawatari, R., Yamaguchi, T., O’Loughlin, F., Neal, J.C., Sampson, C.C.,  
642 Kanae, S., Bates, P.D., 2017. A high-accuracy map of global terrain elevations. *Geophys Res Lett*  
643 44, 5844–5853. <https://doi.org/10.1002/2017GL072874>  
644

645 Yamazaki, D., Kanae, S., Kim, H., Oki, T., 2011. A physically based description of floodplain  
646 inundation dynamics in a global river routing model. *Water Resour Res* 47.  
647 <https://doi.org/10.1029/2010WR009726>  
648

649 Yamazaki, D., Baugh, C.A., Bates, P.D., Kanae, S., Alsdorf, D.E., Oki, T., 2012. Adjustment of a  
650 spaceborne DEM for use in floodplain hydrodynamic modeling. *J Hydrol* 436–437, 81–91.  
651 <https://doi.org/10.1016/j.jhydrol.2012.02.045>  
652

653 Yamazaki, D., O’Loughlin, F., Trigg, M.A., Miller, Z.F., Pavelsky, T.M., Bates, P.D., 2014.  
654 Development of the Global Width Database for Large Rivers. *Water Resour Res* 50, 3467–3480.  
655 <https://doi.org/10.1002/2013WR014664>  
656

657 Yamazaki, D., Ikeshima, D., Sosa, J., Bates, P.D., Allen, G., Pavelsky, T., 2019. MERIT Hydro: A  
658 high-resolution global hydrography map based on latest topography datasets. Water Resour. Res.  
659 2019WR024873. <https://doi.org/10.1029/2019WR024873>  
660